Journal of GeoEngineering, Vol. 18, No. 1, pp. 021-031, March 2023
http://dx.doi.org/10.6310/jog.202303_18(1).3

PERFORMANCE OF GEOTECHNICAL SYSTEMS UNDER EXTREME HYDROCLIMATIC EVENTS USING A NEW USER-DEFINED SOIL MODEL IN PLAXIS

Tharshikka Vickneswaran [1], Nadarajah Ravichandran [2*]

ABSTRACT

Extreme hydroclimatic events such as heavy rainfall and drought have occurred frequently in recent years, and their impacts on geotechnical systems must be understood for developing climate-adaptive design procedures. A fully coupled flow-deformation finite element method is best suited for accurately predicting the behavior of geotechnical structures under extreme hydroclimatic events. PLAXIS, a finite element software widely used by practicing engineers and researchers, models water flow accurately, but the deformation model is not fully coupled with the flow model because the constitutive models do not update the stiffness and failure criterion during water flow. Therefore, to improve the predictive capability, first, the elastic modulus and yield criterion of the Mohr-Coulomb (MC) model was modified, validated, and implemented as a user-defined constitutive model in PLAXIS. Then, the Modified Mohr-Coulomb (MMC) model was used to understand the hydromechanical behavior of foundations and earth slopes under site-specific extreme hydroclimatic events in a coupled manner. The temporal variation of the (a) safety factor of earth slopes, (b) skin and tip resistances and settlement of deep foundations, and (c) settlement of shallow foundations were estimated for the site-specific extreme hydroclimatic events. The results show that the traditional design limits are altered by the hydroclimatic events, and therefore the existing design methods must be updated.

Key words: Unsaturated soil, user-defined soil model, modified cohesion, Mohr-Coulomb model.

1. INTRODUCTION

On a daily average, over the past 50 years, 115 people have been killed, and $202 million has been lost on the damages caused due to extreme hydroclimatic events such as heavy rainfall, flooding, and drought, according to the World Meteorological Organization (WMO 2021). These extreme hydroclimatic events impact the performance of various critical structures such as bridges, buildings, and earth dams and levees. Due to the extreme hydroclimatic events, the amount of water in the unsaturated soils, *i.e.,* the degree of saturation (DoS), varies and affects the strength, deformation, and flow properties of the soils. Such a temporal and spatial variation of the DoS affects the mechanical behavior of soil-supported geotechnical and structural systems. Mahmoudabadi and Ravichandran (2021) proposed a new climate-adaptive design method that considers the site-specific hydroclimatic parameters such as precipitation, evapotranspiration, and water table depth in the design, besides just the traditional geotechnical parameters. Vahedifard *et al.* (2018) discussed how soil-atmospheric interactions and extreme event patterns in a changing climate could alter soil properties and loading conditions, affecting the performance of partially saturated geotechnical structures. Their studies showed the importance of considering the effect of matric suction and the DoS due to extreme hydroclimatic events in the design.

The finite element method has been used widely in geotechnical engineering to understand complex phenomena. For accurate modeling of soil behavior under hydroclimatic events, the finite element model must consider the effects of the DoS in the hydromechanical behavior of soil in a coupled manner. Among the many in-house and commercial finite element programs, PLAXIS is a special-purpose finite element program for modeling many geotechnical engineering systems under complex geometric and thermal, mechanical, and hydrological loading conditions. Although PLAXIS models the flow of water (both influx and outflux) through an unsaturated zone using the Richards equation for coupled-flow deformation analysis, it does not update the deformation parameters such as modulus and yielding due to matric suction and/or DoS variation during a hydroclimatic event. In other words, the constitutive models available in PLAXIS do not incorporate the unsaturated soil mechanics principles. However, this drawback can be overcome by using a constitutive model for unsaturated soil as a user-defined soil model (UDSM) to accurately predict the behavior of geotechnical systems in a fully coupled manner using PLAXIS.

In this study, a simple and widely used linear elastic-perfectly plastic Mohr-Coulomb (MC) model was first modified for unsaturated soil by updating the elastic modulus and yield criterion based on the matric suction and DoS and used within PLAXIS as a user-defined constitutive model. Then, selected geotechnical systems subjected to extreme hydroclimatic events were analyzed in a coupled manner using the modified constitutive model within PLAXIS. The MC model modification, implementation, validation, and verification details and the predicted behavior of geotechnical systems under extreme hydroclimatic events are discussed below.

Manuscript received December 12, 2022; revised February 27, 2023; accepted February 28, 2023.
[1] Assistant Professor, Civil and Environmental Engineering, University of Louisville, Louisville, Kentucky 40208.
[2*] Associate Professor (corresponding author), Glenn Department of Civil Engineering, Clemson University, 202 Lowry Hall, Clemson, SC, 29634 (e-mail: nravic@clemson.edu).

2. MODIFICATION OF MOHR-COULOMB MODEL FOR FULLY COUPLED FLOW-DEFORMATION ANALYSIS

There are many advanced/complex and accurate constitutive models for unsaturated soils in the literature (Alonso *et al.* 1990; Wheeler and Sivakumar 1995; Loret and Khalili 2002). Most of these advanced models require many model parameters, and determining them from traditional laboratory and/or field tests is not easy. It is also observed that most of the advanced elastoplastic constitutive models are computationally expensive and numerically unstable when used within finite element code for coupled flow-deformation analysis (Ravichandran 2009). On the other hand, the MC soil model is a simple and widely used model by practicing engineers and researchers to approximate the nonlinear elastoplastic stress-strain behavior of soils. Also, it is numerically stable within a coupled flow-deformation finite element code compared to other complex and advanced constitutive models.

In general, the development of an elastoplastic constitutive model consists of three major components: (1) yield criterion, (2) plastic flow rule, and (3) strain hardening rule (or work hardening). The MC model consists of an initial linear elastic part until it reaches a specific yield strain or stress value and a perfectly plastic part beyond it. Figure 1 shows the nonlinear stress-strain behavior of a typical soil with hardening and softening parts and its approximation with the linear elastic and perfectly plastic MC model. The initial modulus and the onset of yielding vary with the matric suction and/or DoS of the soil. However, the MC model available in PLAXIS is a traditional model which does not update the modulus and yielding criterion based on the matric suction and/or DoS. To improve the accuracy of the prediction of the coupled flow-deformation module, the MC model was modified by updating the initial modulus and yield criterion as a function of matric suction and/or DoS in this study. The details of the modification are described in detail below.

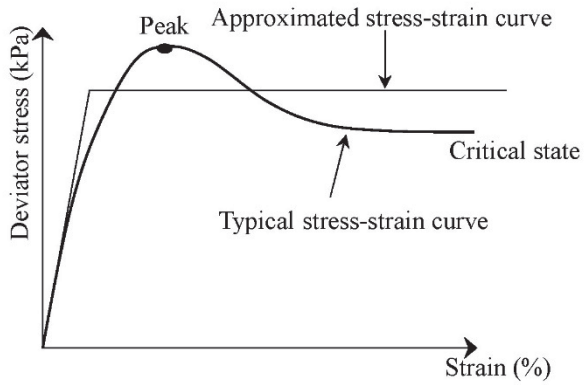

Fig. 1 Typical stress-strain behavior and its approximation using MC model

2.1 Linear Elastic Part

The linear elastic part of the MC model is defined with only two parameters: elastic modulus (E_s) and Poisson's ratio. Although both parameters affect mechanical behavior, only the E_s was updated in this study because of its significance. The variation of E_s under unsaturated conditions can be expressed as a function of the DoS and matric suction. Among the many equations available in the literature (Steensen-Bach *et al.* 1987; Schnaid *et al.* 1995; Costa *et al.* 2003; Oh *et al.* 2009; Vanapalli and Adem 2013), the equation proposed by Oh *et al.* (2009), shown in Eq. (1), was used to update the E_s under unsaturated condition ($E_{s(unsat)}$). The proposed equation is useful to predict the variation of elastic modulus and elastic settlement of unsaturated soils in all three zones: boundary effect, transition, and residual zone of soil water characteristic curve (SWCC).

$$E_{s(unsat)} = E_{s(sat)}\left\{1+\alpha_e(u_a-u_w)S^{\beta_e}\right\} \quad (1)$$

where $E_{s(sat)}$ is the elastic modulus of the soil under the saturated condition at a 1% strain, $(u_a - u_w)$ is the matric suction, α_e and β_e are model parameters and S is the degree of saturation. For coarse- and fine-grained soils, the recommended model parameter β_e equals 1.0 and 2.0, respectively. The model parameter α_e is a function of the plasticity index (I_p) of the soil and can be computed using Eq. (2) (Oh *et al.* 2009).

$$\frac{1}{\alpha_e} = 0.5 + 0.312I_P + 0.109I_P^2; \quad 0 \le I_P \le 12 \quad (2)$$

2.2 Plastic Part and Yield Criterion

According to the MC yield criterion, the soil will yield when the stress combinations satisfy the yield function shown in Eq. (3). The yield function is expressed in terms of principal stresses and the strength parameters: effective friction angle (ϕ') and effective cohesion (c') (PLAXIS 2020). The yield function will be updated by updating the strength parameters as a function of the DoS and/or matric suction.

$$F_s = \frac{1}{2}(\sigma'_1-\sigma'_3)+\frac{1}{2}(\sigma'_1+\sigma'_3)\sin(\phi')-c'\cos(\phi') = 0 \quad (3)$$

2.2.1 Variation of Friction Angle

Several experimental studies have shown that the variation of soil strength with matric suction is nonlinear (Kayadelen 2007; Reis *et al.* 2011; Banerjee 2017, Banerjee *et al.* 2018). Patil *et al.* (2017) showed that the friction angle remained constant for the suction range of 0 to 300 MPa for silty sand. Other studies also showed that the variation of friction angle with matric suction was insignificant (Reis *et al.* 2011; Banerjee 2017; Banerjee *et al.* 2018) for the range of suction (0 to 300 MPa) experienced by the soil in this study and therefore, the effective friction angle was assumed to be constant.

2.2.2 Variation of Cohesion

Literature shows that soil cohesion varies significantly with matric suction (Lu and Likos 2006; Jarast and Ghayoomi 2017; Taylor 1948; Tran and Fredlund 2021; Lin *et al.* 2016) and therefore needs modification. The cohesion under unsaturated conditions is typically calculated by adding the additional cohesive strength to the saturated cohesion. Ho and Fredlund (1982) proposed an equation for total cohesion by adding suction contribution to the traditional effective cohesion, as shown in Eq. (4).

$$c_t = c' + (u_a - u_w)\tan(\phi^b) \quad (4)$$

where c_t is the total cohesion of the soil under unsaturated conditions, including the effect of suction increment, c' is the effective cohesion relative to zero suction, $(u_a - u_w)$ is the matric suction, $\tan(\phi^b)$ is the slope of the failure line representing the change in soil shear strength due to change in soil suction. Another equation (Eq. (5)) was proposed by Kayaleden (2007) to estimate the cohesion at different suction for clayey soils by adding additional cohesion due to suction.

$$c_t = c' + (u_a - u_w)_b \tan(\phi') \ln\left[\frac{(u_a - u_w) + P_{atm}}{P_{atm}}\right] \quad (5)$$

where c_t is the total cohesion of the soil, c' is the effective cohesion relative to zero suction, $(u_a - u_w)$ is the matric suction, $(u_a - u_w)_b$ is the air entry value of the soil, ϕ' is the traditional effective friction angle, and P_{atm} is the atmospheric pressure. According to the developers (Kayaleden 2007), this equation is suitable for computing the total cohesion of clayey soils.

In this study, a general equation that can be applicable to a wide range of soils was developed, overcoming the limitations of the previous equations. Previous studies show that the variation of cohesion with matric suction follows logarithmic function (Kayadelen 2007; Reis *et al.* 2011; Banerjee 2017). Therefore, in this study, the relationship between total cohesion (c_t) and suction (ψ) is described in the suction and logarithm of the cohesion plane with variables A and B, as shown in Eq. (6).

$$c_t = A + B \log(\psi) \quad (6)$$

However, when the matric suction is zero, c_t should be equal to c' at saturated state. Also, substituting zero for suction for the saturated condition, the log term has no mathematical meaning. Therefore, suction was normalized by first adding the atmospheric pressure and then devising it by atmospheric pressure to eliminate this error, as shown in Eq. (7).

$$c_t = A + B \log\left(\frac{\psi + P_{atm}}{P_{atm}}\right) \quad (7)$$

It can be seen that in Eq. (7), the variable A becomes c' when the soil is fully saturated (zero suction). Then, by carefully studying the total cohesion values for several soils at different suction values (Farouk *et al.* 2004; Reis *et al.* 2011; Banerjee 2017; Patil *et al.* 2017; Banerjee *et al.* 2018; Awad and Sasankul 2018) and considering the fact that the unsaturated soil properties could be related to the soil water characteristic model parameters, a new equation for B as a function of SWCC model parameters (g_n, θ_r, and n) was proposed, as shown in Eq. (8).

$$B = g_n\left(\frac{\theta_r}{n}\right) \quad (8)$$

where θ_r is the residual water content, n is the porosity, and g_n is a model parameter which is the same as one of the model parameters of van Genuchten soil-water characteristic curve. The final equation for the total cohesion is expressed as a function of matric suction, porosity, residual water content, and g_n, as shown in Eq. (9).

$$c_t = c' + g_n\left(\frac{\theta_r}{n}\right)\log\left(\frac{\psi + P_{atm}}{P_{atm}}\right) \quad (9)$$

The stress-strain behavior of most soils under unsaturated conditions can now be represented by the modified elastic modulus and cohesion models. One may use the θ_r and g_n values proposed by Carsel and Parrish (1988) for many types of soils. The validations of the proposed total cohesion and the accuracy of the Modified Mohr-Coulomb (MMC) model are presented in the following sections.

2.3 Validation of MMC Model

The new unsaturated cohesion was incorporated in the deviator stress at failure, as shown in Eq. (10).

$$\Delta\sigma_{df} = \sigma'_1 - \sigma'_3 = \left[c_t\left(\frac{1}{\tan(\phi')}\right) + \sigma'_3\right]\left(\frac{2\sin(\phi')}{1-\sin(\phi')}\right) \quad (10)$$

The stress-strain relationship was calculated using the modified cohesion at different suction values and compared with that available in the literature (Farouk *et al.* 2004; Reis *et al.* 2011; Banerjee 2017; Patil *et al.* 2017; Awad and Sasanakul 2018).

Farouk *et al.* (2004) presented the results of a series of triaxial tests on siliceous sand that consisted of nearly 7.0% fine sand and 93.0% medium sand. Figure 2 shows the experimental deviator stress vs. strain obtained from Farouk *et al.* (2004) at matric suction values of 0, 30, 50, and 150 kPa. The variation of deviator stress with strain at different matric suction predicted from Eq. (10) is graphically compared with those measured values from Farouk *et al.* (2004) in Fig. 2. The comparison shows a good agreement between the predicted and measured values for sands, and the linear elastic-perfectly plastic model captures the overall behavior of the sandy soil well.

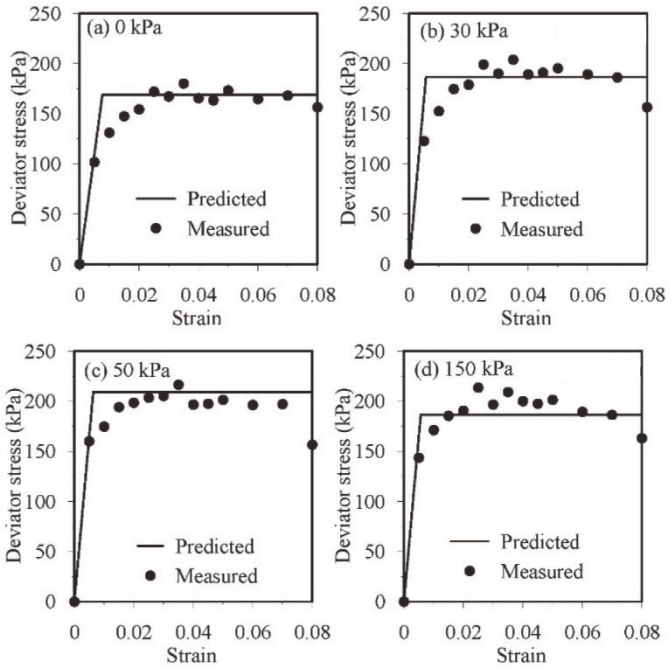

Fig. 2 Comparison of measured (data recreated from Farouk *et al.* 2004) and predicted stress-strain behaviors at the suction values of (a) 0 kPa, (b) 30 kPa, (c) 50 kPa, and (d) 150 kPa

Banerjee (2017) presented the results of a series of triaxial tests conducted on unsaturated silt soil of low plasticity (ML). The deviatoric stress vs. strain curve of the unsaturated specimens during shearing in drained conditions at matric suction values of 0, 50, 250, and 750 kPa is shown in Fig. 3. The variation of deviator stress with strain at different matric suction predicted from Eq. (10) is graphically compared with those measured values from Banerjee (2017) in Fig. 3. The results indicated a good comparison between those predicted and the measured values for silty soil.

Reis *et al.* (2011) conducted a triaxial test program in soil specimens (SC-SM) in saturated and unsaturated conditions. It is presented and compared with results from conventional triaxial tests. Matric suction values of 80 and 160 kPa and net confining stresses of 50 kPa, 100 kPa, and 150 kPa were used. The soil was classified as SC-SM according to ASTM D2487-00. The variation of deviator stress with strain at confining stress of 100 kPa and matric suctions of 0, 80, and 160 kPa predicted from Eq. (10) is compared with those measured values by Reis *et al.* (2016) in Fig. 4. The results indicated a good comparison between those predicted and the measured values for SC-SM soil.

Awad and Sasanakul (2018) presented the stress-strain behavior of compacted clayey sand measured using constant water content triaxial tests. The variation of deviator stress with strain at matric suctions of 50, 100, and 200 kPa predicted from Eq. (10) is compared with those measured values by Awad and Sasanakul (2019) in Fig. 5. The results indicated a good comparison between those predicted and the measured values for clayey soil.

Patil *et al.* (2017) presented the results of suction-controlled triaxial tests conducted between 0.05 MPa to 300 MPa suction range on silty sand. Their results show the stress-strain behavior for confining pressure of 300 kPa at different matric suction values of 0, 50 kPa, 250 kPa, 500 kPa, 750 kPa, 20 MPa, and 300 MPa was plotted in Fig. 6. The experimental values were compared with the values predicted from the proposed model. It should be noted that from suction values 0 kPa to 750 kPa, there is a good agreement in the stress-strain behavior. But in the case of higher suction values like 20 MPa the predicted values are higher than the experimental values, and for 300 MPa the predicted values are lower than the observed values. Therefore, the proposed empirical model is limited to 750 kPa of matric suction.

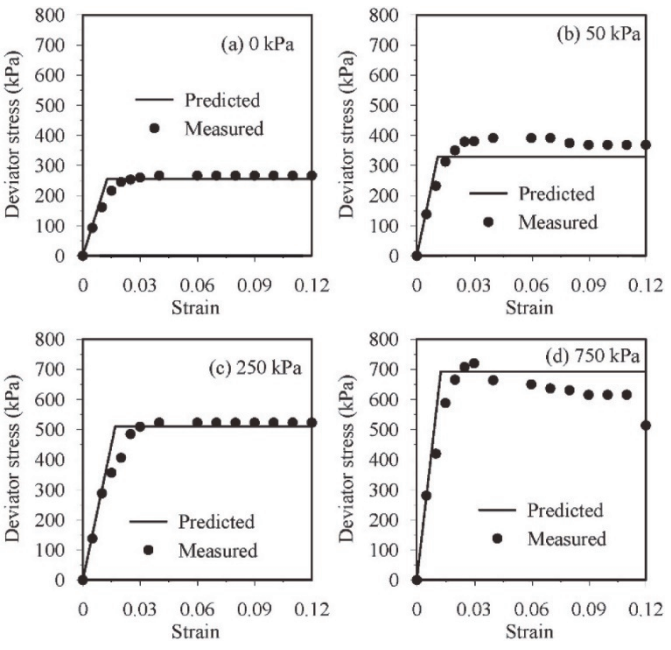

Fig. 3 Comparison of measured (data recreated from Banerjee 2017) and predicted stress-strain behaviors at suction values of (a) 0 kPa, (b) 50 kPa, (c) 250 kPa, and (d) 750 kPa

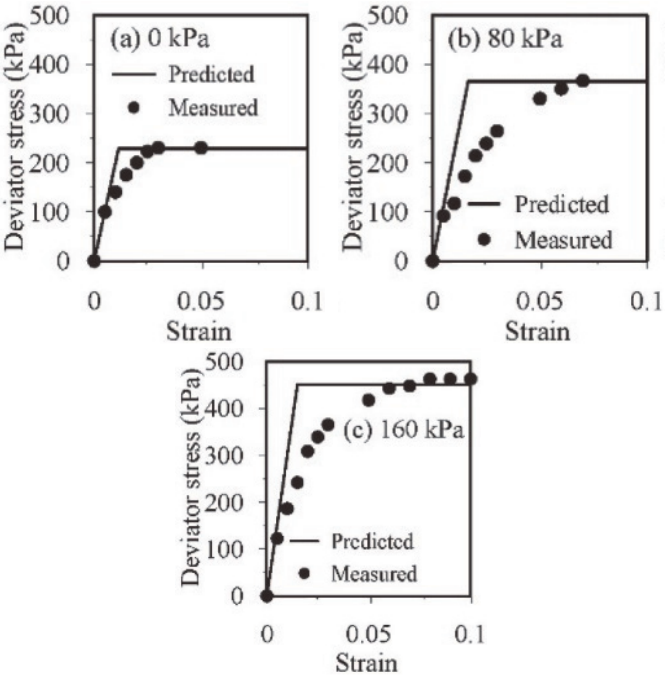

Fig. 4 Comparison of measured (data recreated from Reis *et al.* 2011) and predicted stress-strain behaviors at suction values of (a) 0 kPa, (b) 80 kPa, and (c) 160 kPa

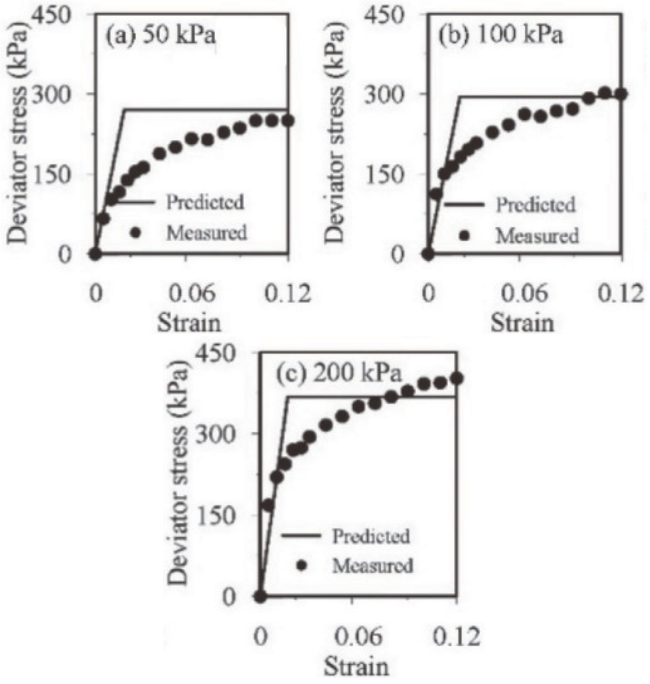

Fig. 5 Comparison of measured (data recreated from Awad and Sasanakul 2018) and predicted stress-strain behaviors at suction values of (a) 50 kPa, (b) 100 kPa, and (c) 200 kPa

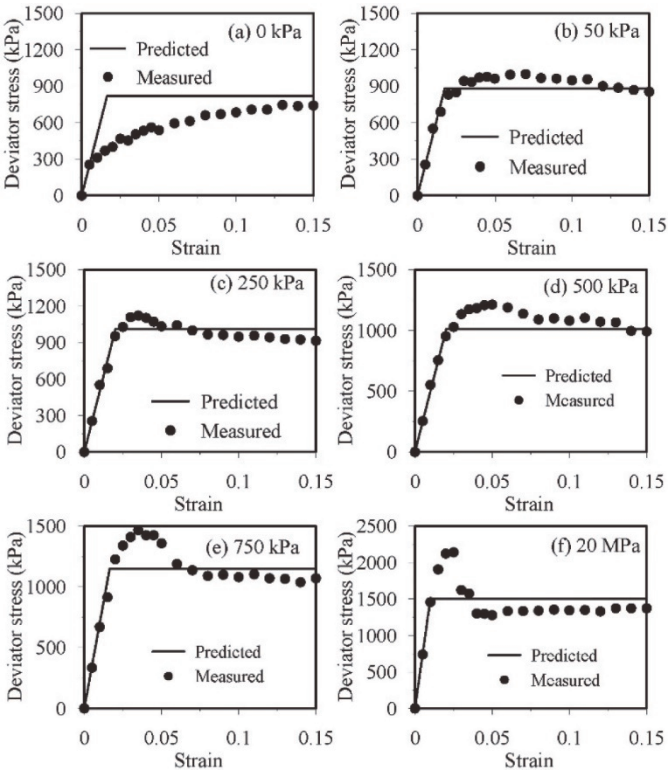

Fig. 6 Comparison of measured (data recreated from Patil *et al.* 2017) and predicted stress-strain beahviors at suction values of (a) 0 kPa, (b) 50 kPa, (c) 250 kPa, (d) 500 kPa, (e) 750 kPa, and (f) 20 MPa

2.4 Effect of Model Parameters

The effect of model parameters n, θ_r, and g_n in the proposed Eq. (9) was investigated for its application to different types of soils by varying them within the range for common soils. The parametric study results for n, θ_r, and g_n are shown in Figs. 7(a), 7(b), and 7(c), respectively. From the results, it was observed that the total cohesion decreased with increasing n and increased with g_n and θ_r.

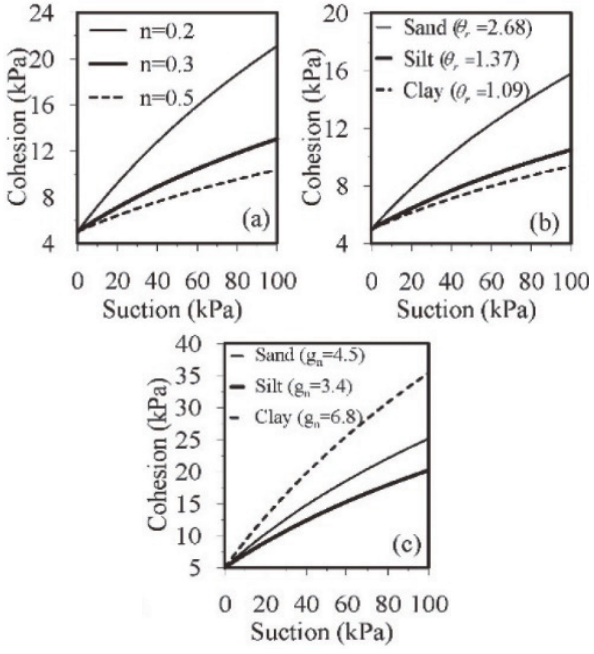

Fig. 7 Effect of model parameters (a) n, (b) g_n, and (c) θ_r on the variation of cohesion with matric suction

3. IMPLEMENTATION OF UDSM IN PLAXIS

The implementation of the new constitutive model within PLAXIS as a UDSM involved major modification of two subroutines provided within the software and the development of a new subroutine compatible with the software. The subroutine USRADDF.for was modified to add additional model parameters needed for using the modified MC model. This subroutine interacts with the software graphical user interface (GUI) and displays the parameter with spaces for entering the data as inputs. The subroutine User_Mod.for, that interacts with the calculation phase, was used to access the DoS/matric suction at every iteration for updating the field variables. Then, a new subroutine called MC.for was developed to update the elastic modulus and failure criterion and to calculate the matrices and vectors before solving the dynamic equilibrium equations. The four subroutines USRADDF.for, User_Mod.for, LIBRARY.for, and MC.for were compiled to generate a DLL file. Finally, the DLL was placed in the UDSM directory in PLAXIS for using the new MMC model as a UDSM.

4. VERIFICATION OF THE MODEL IMPLEMENTATION

Verification of the MMC model implemented through the UDSM was performed by applying a static load to the soil domain with different initial degrees of saturation. The properties of the sandy soil listed in Table 1 were used in the analyses. The corresponding van Genuchten SWCC model parameters corresponding to the sandy soils obtained from the PLAXIS manual are shown in Table 1. The model parameters used for calculating the modulus of elasticity and failure in the MMC model are shown in Table 2.

Table 1 General and hydraulic soil properties

General properties	Value	Hydraulic properties	Value
Saturated unit weight γ_{sat} (kN/m^3)	21.72	Residual degree of saturation	0.2
Dry unit weight γ_{dry} (kN/m^3)	18.91	Saturated degree of saturation	1.00
Void ratio (e)	0.40	Fitting parameter g_n	1.51
Poisson's ratio (v)	0.30	Fitting parameter g_a (1/m)	1.32
Effective friction angle c' (°)	33	Saturated elastic modulus (E) (MPa)	30
Effective cohesion ϕ' (kPa)	5	Hydraulic conductivity (m/day)	1.00

Table 2 MMC model parameters

Model parameters	Value
Fitting parameter α	2.00
Fitting parameter β	1.00
Residual water content θ_r(%)	0.69
Porosity n	0.29
Fitting parameter g_n	1.51

4.1 Finite Element Model and Analysis

Verification involved applying a static line load of 150 kN/m for a soil domain of depth 10 m and width 20 m, as shown in Fig.

9. The MMC model was verified with the Traditional Mohr-Coulomb (TMC) model by using the properties shown in Tables 1 and 2. The plastic analysis with different initial degrees of saturation without the flow effect was considered for the verification. The cohesion and modulus of elasticity values were calculated at different degrees of saturation and corresponding matric. Then, the values were inputted into the TMC model in PLAXIS. The values were calculated for inputting in TMC since the effect of matric suction and/or degree of saturation is not considered in calculating modulus and cohesion in PLAXIS 2D. However, in the MMC model, the values were automatically calculated depending on the matric suction and degree of saturation through the UDSM. The variation of vertical displacement at different degrees of saturation obtained from MMC coincided well with the values obtained from TMC.

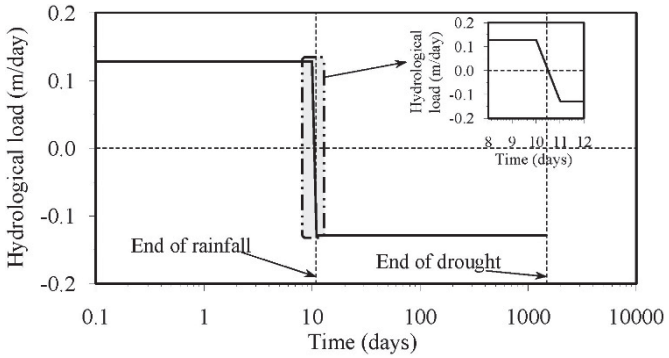

Fig. 8 Hydroclimatic load-time history

5. APPLICATIONS OF THE PROPOSED CONSTITUTIVE MODEL WITHIN PLAXIS

The implemented MMC was used to investigate the impacts of extreme hydroclimatic events on the settlement behavior of shallow foundations, skin and tip resistances of deep foundations, and stability of earth slopes.

5.1 Hydroclimatic Load

According to the U.S. Drought Monitor, the longest duration of drought in California lasted 376 weeks from the end of 2011 to 2019. Therefore, in this study, 4 years of extreme drought with an outflow intensity of 0.13 m/day was considered to simulate the extreme drought condition. On the other hand, a 10-day rainfall with an inflow intensity of 0.13 m/day was considered to simulate the heavy rainfall, as shown in Fig. 8. The rainfall was applied using the inflow boundary condition drought was applied using the outflow boundary condition.

5.2 Variation of Settlement of Shallow Foundation Subjected to Hydroclimatic Events

The settlement of the shallow foundations, which is the key parameter for the geotechnical design, is usually calculated assuming the soil is fully saturated. However, the near-surface soil is unsaturated during seasonal variation and climate change. Such changes in suction and/or DoS can affect the settlement behavior of shallow foundations (Ravichandran *et al.* 2021). To gain better insights into the impacts of extreme hydroclimatic events, the settlement behavior of the shallow foundation was investigated using the MMC implemented in PLAXIS with the flow model in a coupled manner.

5.2.1 Finite Element Model and Analysis

A two-dimensional plane strain model of a 1 m wide continuous foundation placed at the ground surface, as shown in Fig. 9, was created and analyzed using PLAXIS. The simulation domain was spatially discretized using 15-Node triangular elements. The deformation and groundwater flow boundaries were assigned to the model to match the field conditions. The deformation in the x-direction is restrained along the left and right vertical boundaries and in both x- and y-directions along the base. The flow through the base and vertical sides was restricted by applying closed flow boundary conditions. The mesh was refined around the foundation, where stress, deformation, and/or flow are concentrated to capture the high gradients accurately. Size and mesh sensitivity studies were performed to select the size of the simulation domain (20 m $\times$ 10 m) such that the computed results are not affected by the size and the mesh selection. The geotechnical properties and the constitutive model parameters are shown in Tables 1 and 2. The extreme drought was assumed as the initial condition for the analysis, with an initial DoS of 20% and corresponding suction of 218 kPa. First, the mechanical load shown in Fig. 9 was applied, and then the hydroclimatic load shown in Fig. 8 was applied to the model.

5.2.2 Results and Discussion

The rainwater infiltrated to a depth of 2 m (influence zone) at the end of 3.25 days, as shown in Fig. 10(a). The results indicated that the initial DoS of 20% reached a maximum value of 91.3% at a depth of 1, and 2 at the end of 1.36, and 3.25 days, respectively. The wetting front moved to a depth of 6.25 m at the end of ten days of rainfall, as shown in Fig. 10(b). The DoS at the ground surface reduced to 30% at the end of the drought phase, as shown in Figs. 10(c) and 11(a). From these figures, it is evident that the wetting front reached the bottom of the influence zone (2 m below the bottom of the footing) at the end of 3.25 days. Figure 11(b) shows the soil continued to settle until 3.25 days when the wetting front reached the influence zone. The soil began to heave after 3.25 days and then began to settle once the rainfall stopped after 10 days. The results indicated that the shallow foundation experienced significant settlement and heaving due to the simulated extreme hydroclimatic events.

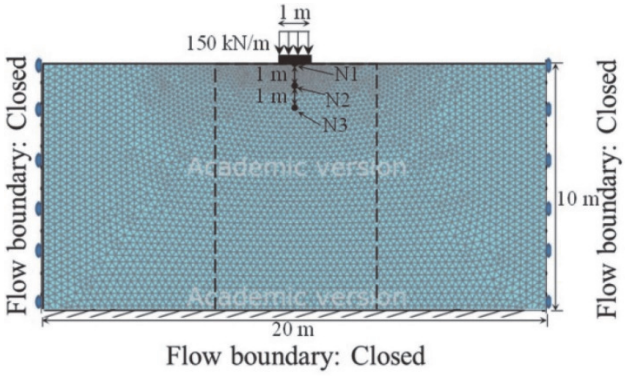

Fig. 9 Simulation domain and finite element mesh

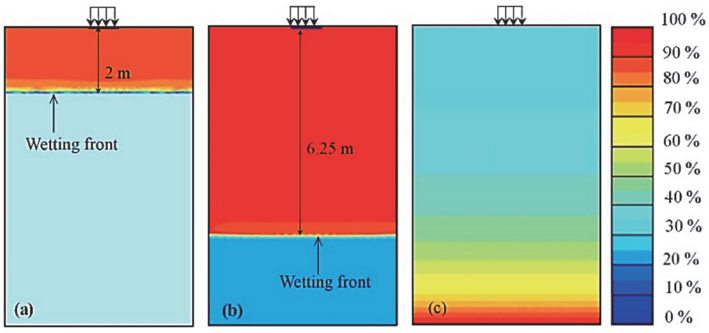

Fig. 10 Degree of saturation contours at the end of (a) 3.25 days, (b) 10 days of rainfall, and (c) 4 years of drought

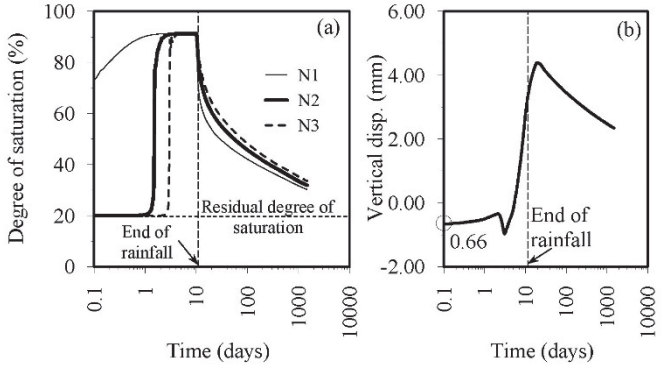

Fig. 11 (a) Degree of saturation-time history and (b) vertical displacement-time history below the center of the foundation

5.3 Variation of Skin and Tip Resistances of Drilled Shaft Subjected to Hydroclimatic Events

The skin and tip resistances contribute to the axial capacity of a deep foundation. The variation in soil properties around the skin and tip can affect not only the settlement behavior but also the axial capacity of the foundation. The impacts of extreme hydroclimatic events on the skin and tip resistances and settlement behavior of a deep foundation were investigated using the proposed constitutive model within PLAXIS in a coupled manner, and the results are presented in the next section.

5.3.1 Finite Element Model and Analysis

A deep foundation with a diameter of 1 m and length of 12 m subjected to axial load, as shown in Fig. 12, was considered in this study. The two-dimensional axisymmetric formulation was used to model the soil and drilled shaft. The foundation was modeled using non-porous linear elastic material with a modulus of 24.8 GPa. The simulation domain was spatially discretized using 15-Node triangular elements. The flow and deformation boundary conditions described in the analysis of shallow foundation was used. The mesh was refined around the foundation where stress, deformation, and/or flow are concentrated to capture the high gradients accurately. A size and mesh sensitivity study was performed to select the size of the simulation domain (40 m × 20 m) such that the computed results are not affected by the size and the mesh selection. The soil and the constitutive model parameter are tabulated in Tables 1 and 2. The subsurface was assumed to be dry with an initial DoS of 20% and corresponding suction of 218 kPa. The initial skin and tip resistances were calculated as 1964.34 kN (β method) and 827.66 kN (Meyerhof 1963), respectively, using analytical equations available in the literature. The ultimate capacity of 1396 kN was calculated using a factor of safety of 2. This concentrated load was converted into a surface load of 1777.4 kN/m^2 and applied to the foundation for the plane strain numerical analysis. First, the mechanical load shown in Fig. 12 was applied, and then the hydroclimatic load shown in Fig. 8 was applied to the model.

5.3.2 Results and Discussion

The variation of the vertical displacement and axial force are shown in Figs. 13(a) and 13(b), respectively. Since the surface load was applied on the foundation, the vertical displacement and vertical stress contours across the width of the foundation were similar (no bending due to numerical error was observed). Therefore, the displacements and forces computed at the center of the foundation were considered representative of the foundation. The variation of vertical displacement due to the mechanical load of 1396 kN induced in the foundation is shown in Figs. 14(a) and 14(b), with initial degrees of saturation of 20% and 100%, respectively. The results indicated that the vertical displacement was higher for the initial DoS of 100% than 20%. It is due to the high matric suction for 20% initial DoS.

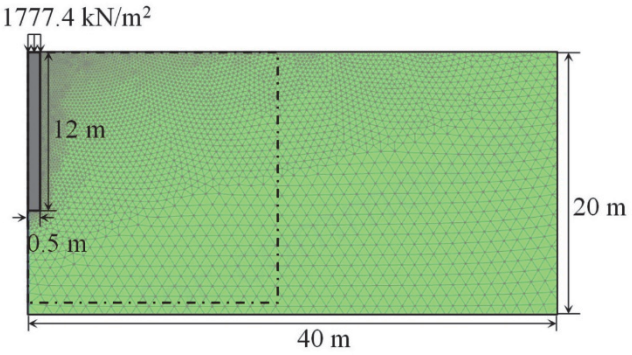

Fig. 12 Simulation domain and finite element mesh

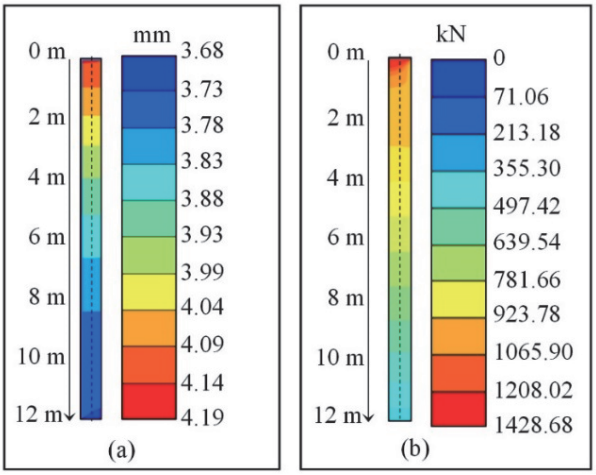

Fig. 13 Contours for (a) vertical displacement and (b) axial force subjected to mechanical load

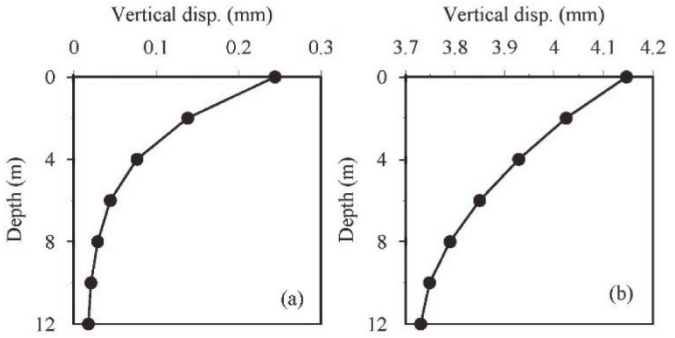

Fig. 14 Deformation profile of the pile subjected to mechanical load with uniform initial degrees of saturation of (a) 20% and (b) 100%

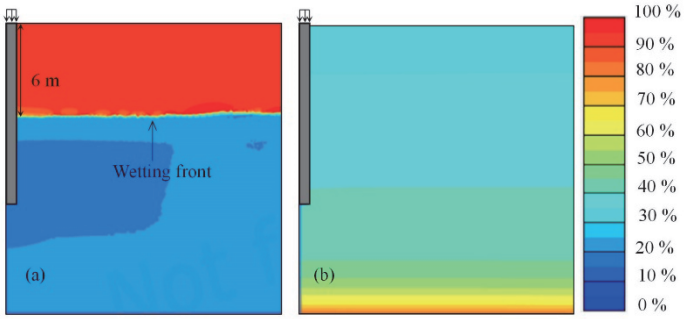

Fig. 15 Degree of saturation contours at the end of (a) 10 days of rainfall and (b) 4 years of drought

The effect of hydroclimatic events on the behavior of the foundation was analyzed by applying the hydroclimatic load shown in Fig. 8. Figures 15(a) and 15(b) show the DoS contours at the end of 10 days of rainfall and 4 years of drought for the area enclosed by the dotted line in Fig. 12. Figure 16(a) shows the DoS-time history at the pile head, middle of the pile, and pile tip. The results indicated that the wetting front reached a depth of 6 m at the end of 10.5 days of rainfall. The DoS decreased and reached a minimum value of 29.4% near the top of the foundation at the end of the drought. Figure 16(b) shows the maximum settlement of 0.0087 mm at the pile head due to the hydroclimatic event. The pile head moved down (settled) during rainfall and moved up (heaved) once the drought phase started to a maximum value of 0.044 mm.

The mechanical load of 1777.4 kN/m^2 induced a maximum axial force of 1396.2 kN and 238.95 kN in the pile head and tip, respectively. Figure 17 shows the variation of axial force in the foundation due to the mechanical load. From the figure, it was observed that the skin resistance developed in the pile due to the mechanical load was 1188.3 kN, for the initial DoS was 20%. The axial forces at the top and the bottom of the foundation were 1401.67 kN and 229.66 kN, respectively, for the initial DoS was 100% (fully saturated condition). Therefore, the skin resistance for the initial DoS was 100% was 1172.01 kN. This shows that the skin resistance with the initial DoS of 20% (suction = 218 kPa) was higher than that for the initial DoS of 100%.

Figure 18 shows the axial force induced in the pile at the end of rainfall (10.5 days), 100 days, and drought (1470 days). The significant difference in the axial force along the foundation was observed at a depth of 2-10 m. The results showed that the axial force induced due to rainfall increased due to the drought (at the end of 100 days). The maximum axial force distribution was obtained at the end of the drought phase.

Figure 19 shows the variation of skin resistance with time. The results indicated that the skin resistance reduced when the water infiltrated and increased once the drought phase began. Again, the skin resistance reduced after 100 days when the DoS near the pile tip increased to 58%, as shown in Fig. 19. This shows the increase in the resistance given by the soil due to the increase of matric suction caused by drought. The skin resistance reached a maximum value of 1080.60 kN at the end of 100 days of the hydroclimatic event.

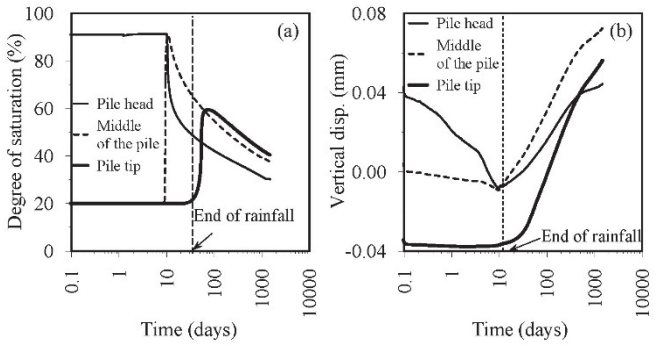

Fig. 16 (a) Degree of saturation-time histories at selected depths and (b) settlement-time histories at selected depths subjected to hydroclimatic

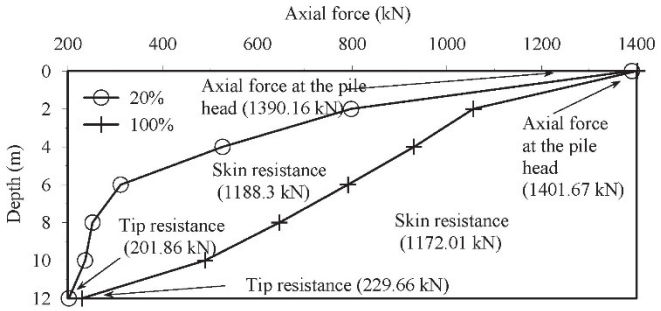

Fig. 17 Axial force distribution in the pile subjected to mechanical load with uniform initial degrees of saturation of (a) 20% and (b) 100%

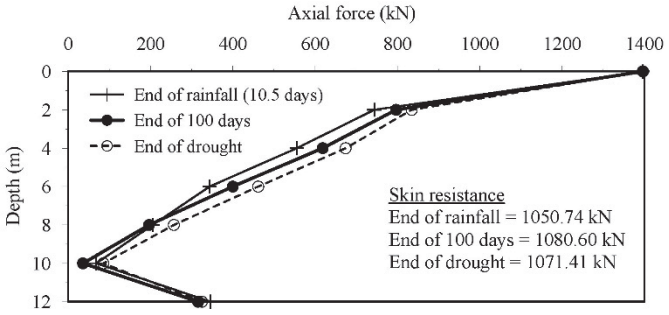

Fig. 18 Axial force distribution in a pile at the (a) end of rainfall (10.5 days), (b) end of 100 days, and (c) end of rainfall and drought

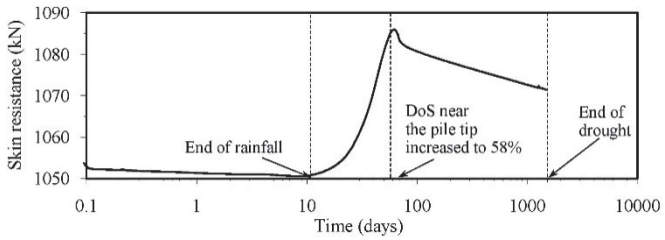

Fig. 19 Variation of skin resistance due to hydroclimatic loads

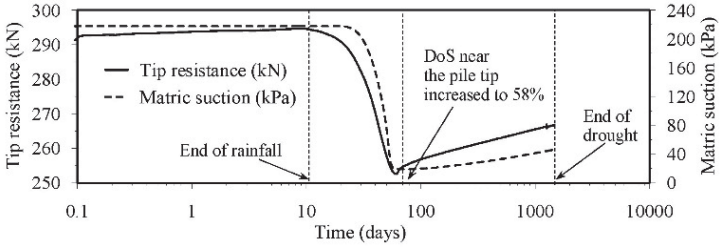

Fig. 20 Variation of tip resistance due to hdyrological loads

Figure 20 shows the variation of tip resistance due to hydroclimatic loads. The matric suction and tip resistance were almost constant until around 20 days because the wetting front was above the tip of the pile. Then, it began to decrease due to the movement of the wetting front within the influence zone below the tip. The decrease in tip resistance continued until it reached the lowest value of 252.4 kN at around 60 days. The tip resistance increased during the drought phase when the matric suction increased, and the tip resistance reached 266.8 kN at the end of the drought. The results indicated that the skin resistance and tip resistance of the pile changed significantly due to extreme hydroclimatic events.

5.4 Variation of Safety Factor of Earth Slopes subjected to Hydroclimatic Loads

This section deals with the stability and deformation behavior of the earth slope subjected to the extreme hydroclimatic event. The slope with a slope ratio of 1.5H: 1V was used for the analysis. The MMC constitutive model within PLAXIS in a coupled manner was used. The details of the analysis are described below.

5.4.1 Finite Element Model and Analysis

A two-dimensional plane strain model was used to represent the earth slope shown in Fig. 21 in PLAXIS 2D. The simulation domain was discretized spatially using 15-node triangular plane strain elements, and the mesh near the slope was refined for accurate results. The deformation boundaries used in the analysis restrain deformations of the vertical sides against translation in the horizontal direction and the base of the model against translation in both horizontal and vertical directions. The flow boundaries were assigned such that the flow through the base and vertical sides of the domain was restricted by applying closed flow boundary conditions. The soil properties and constitutive model parameters tabulated in Tables 1 and 2 were used for the analysis. The analysis of the slope subjected to the extreme hydroclimatic event was carried out by applying the hydroclimatic load-time history shown in Fig. 8 on the top boundaries that include horizontal ground surfaces and slope face.

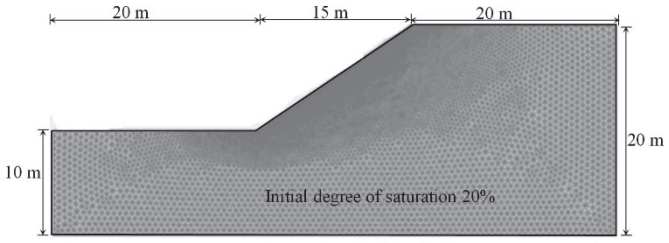

Fig. 21 Simulation domain and finite element mesh

5.4.2 Results and Discussion

A factor of safety (FoS) of 6.16 was obtained for the initial condition. The temporal variation of FoS is shown in Fig. 22, which indicates that the FoS dropped drastically at the end of four days. This is because the wetting front reached the critical failure surface at the end of four days. Figure 23 shows the critical failure surfaces obtained at the initial stage and at the end of four days of rainfall. The wetting front reached the failure surface at the end of four days due to rainfall which may have caused the sudden drop in the FoS at the end of four days.

The initial FoS of 6.16 for the slope reduced to 1.816 at the end of rainfall (at the end of 10 days). This change can be related to the decrease of suction to 0, resulting in a loss of strength in the soil due to the values of modulus and cohesion becoming equal to the saturated modulus and cohesion. At the end of 10 days, the FoS reached a value of 1.65. This variation of FoS indicates the reason for prolonged heavy rainfall inducing slope failures in slopes that stay strong for many years. Then, the FoS began to increase once the drought phase began. The FoS increased to 3.14 at the end of the drought phase, as shown in Fig. 22. Figure 24 compares the critical failure surface obtained at the end of the drought phase with the initial critical failure surface. The results indicated that the critical failure surface deepened during the drought phase compared to the critical failure surface at the end of four days of rainfall. But the critical failure surface at the end of four days was

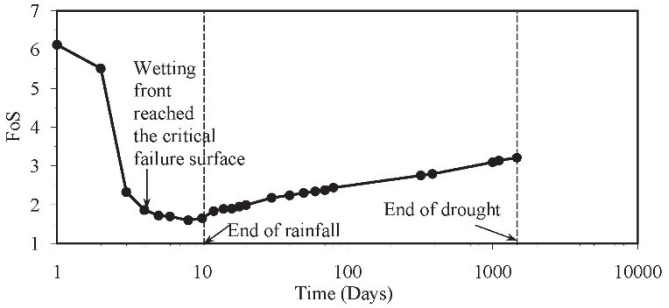

Fig. 22 FoS-time history

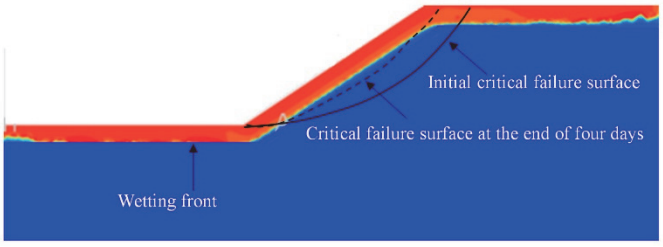

* Color red = 100% degree of saturation and blue = dry (zero)

Fig. 23 Comparison critical failure surfaces predicted before and after four days of rainfall

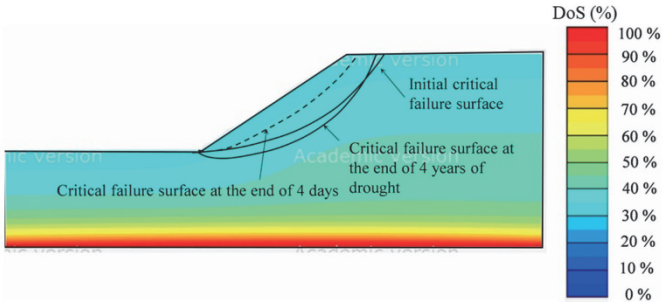

Fig. 24 Comparison critical failure surfaces predicted before, at the end of 4 days of rainfall, and at the end of 4 years of drought

shallower than the initial critical failure surface, as the DoS in the critical failure surface was 30% due to drought, which is higher than the initial DoS of 20%. The results indicated that the FoS dropped drastically due to the extreme rainfall.

6. CONCLUSIONS

In this study, a MMC model along with fully coupled flow was used to analyze the deformation and stability behavior of different geotechnical engineering problems. The settlement behavior of shallow foundations subjected to hydroclimatic events indicated that the soil heaved due to rainfall and settled once the drought phase started. The settlement behavior of the pile indicated that the settlement of the pile head increased with the rainfall. The skin resistance of the pile decreased during the rainfall phase and increased during the drought phase. The stability analysis of the earth slope indicated that the FoS at the start (6.16, 58%) dropped drastically to 1.816 when the wetting front due to rainfall reached the critical failure surface. The observation from the stability analysis indicated the reason for the slope failures subjected to prolonged extreme rainfall. Therefore, the developed model can predict the increased strength and stiffness due to the soil suction in unsaturated soils. Also, the implemented model can be used to predict the temporal and spatial variation of the strength and stiffness of the soil during extreme hydroclimatic events.

It should be noted that the examples presented in this paper considered only a single set of soil properties and mechanical and hydroclimatic loads. It is recommended to consider the variations in soil properties and loads to produce representative results for the site. Such analysis can be conducted using the proposed constitutive model and finite element modeling approach combined with probabilistic analysis procedures.

FUNDING

The authors received no funding for this work.

DATA AVAILABILITY

All data, models, and code generated or used during the study appear in the submitted article.

CONFLICT OF INTEREST STATEMENT

The authors declare that there is no conflict of interest.

REFERENCES

Alonso, E., Gens, A., and Josa, A. (1990). "A constitutive model for partially saturated soils." *Géotechnique*, **40**(3), 405-430. https://doi.org/10.1680/geot.1990.40.3.405

Athapaththu, A., Tsuchida, T., and Kano, S. (2014). "A new geotechnical method for natural slope exploration and analysis." *Natural Hazards*, **75**(2), 1327-1348. http://doi.org/10.1007/s11069-014-1384-0

Awad, M. and Sasanakul, I. (2019). "Shear-induced matric suction in unsaturated clayey sand during constant water content triaxial tests." *Geo-Congress 2019: Geotechnical Materials, Modeling, and Testing*, Meehan CL, Kumar S, Pando MA and Coe JT, Eds. American Society of Civil Engineers, Reston, VA, USA, 853-862. https://doi.org/10.1061/9780784482124.086

Banerjee, A. (2017). *Response of Unsaturated Soils under Monotonic and Dynamic Loading over Moderate Suction States*. Doctoral Dissertation, Arlington, TX: The University of Texas at Arlington. http://hdl.handle.net/10106/26940

Banerjee, A., Puppala, A.J., Patil, U.D., Hoyos, L.R., and Bhaskar, P. (2018). "A simplified approach to determine the response of unsaturated soils using a multistage triaxial test." *IFCEE 2018*, 332-342. https://doi.org/10.1061/9780784481585.033

Chen, F.H. (1988). *Foundations on Expansive Soils*, Elsevier, New York.

Dang, H.P., Lin, H.D., and Hsieh, Y.M. (2010). "Simulation of advanced soil models by using user-defined model feature in PLAXIS." *Proceedings of the 17th Southeast Asian Geotechnical Conference*, Taipei, Taiwan. 149-152.

Duncan, J.M. and Chang, C.Y. (1970). "Nonlinear analysis of stress and strain in soils." *Journal of the Soil Mechanics and Foundations Division*, ASCE, **96**(5), 637-659. https://doi.org/10.1061/JSFEAQ.0001458

Farouk, A., Lamboj, L., and Kos, J. (2004). "Influence of matric suction on the shear strength behavior of unsaturated sand." *Acta Polytechnica*, **44**(4). https://doi.org/10.14311/590

Han, B., Cail, G., Xie, L., Li, J., and Zhao, C. (2020). "Bounding surface constitutive model for unsaturated soils considering microscopic pore structure and bonding effect." *E3S Web of Conferences*, 195, 02007. https://doi.org/10.1051/e3sconf/202019502007

Hsieh, P.G., Ou, C.Y., and Liu, H.T. (2008). "Basal heave analysis of excavations with consideration of anisotropic undrained strength of clay." *Canadian Geotechnical Journal*, **45**, 788-799. https://doi.org/10.1139/T08-006

Kayadelen, C., Tekinsoy, M., and Taşkıran, T. (2007). "Influence of matric suction on shear strength behavior of residual clayey soil." *Environmental Geology*, **53**(4), 891-901. https://doi.org/10.1007/s00254-007-0701-2

Kung, T.C., Hsiao, C.L., and Juang, C.H. (2007). "Evaluation of a simplified small strain model for analysis of excavation induced movements," *Canadian Geotechnical Journal*, **44**(6), 726-736. https://doi.org/10.1139/t07-014

Loret, B. and Khalili, N. (2002). "An effective stress elastic–plastic model for unsaturated porous media." *Mechanics of Materials*, **34**(2), 97-116. https://doi.org/10.1016/S0167-6636(01)00092-8

Mahmoudabadi, V. and Ravichandran, N. (2021). "Climate-adaptive design approach for embedded footing under extreme climate event." *International Journal for Numerical and Analytical Methods in Geomechanics*, **45**(10), 1437-1457. https://doi.org/10.1002/nag.3208

Meyerhof, G.G. (1963). "Some recent research on the bearing capacity of foundations." *Canadian Geotechnical Journal*, **1**(1), 16-26. https://doi.org/10.1139/t63-003

Patil, U.D., Puppala, A.J., Hoyos, L.R., and Pedarla, A. (2017). "Modeling critical-state shear strength behavior of compacted silty sand via suction-controlled triaxial testing." *Engineering Geology*, **231**(21-33). https://doi.org/10.1016/j.enggeo.2017.10.011

Ravichandran, N., Vickneswaran, V., Marathe, S., and Saketh Jella, V. (2021). "Numerical Analysis of Settlement Response of Shallow Footing Subjected to Heavy Rainfall and Flood Events," *International Journal of Geosciences*, **12**(2), 138-158, DOI: 10.4236/ijg.2021.122009.

Reis, R., de Azevedo, R., Botelho, B., and Vilar, O. (2011). "Performance of a cubical triaxial apparatus for testing saturated and unsaturated soils." *Geotechnical Testing Journal*, **34**(3), 103256. https://doi.org/10.1520/gtj103256

Robert, D. (2017). "A modified mohr-coulomb model to simulate the behavior of pipelines in unsaturated soils." *Computers And Geotechnics*, **91**, 146-160. https://doi.org/10.1016/j.compgeo.2017.07.004

Vahedifard, F., Williams, J.A., and AghaKouchak, A. (2018). "Geotechnical engineering in the face of climate change: role of multi-physics processes in partially saturated soils." *IFCEE 2018*. https://doi.org/10.1061/9780784481585.035

Vickneswaran, T. and Ravichandran, N. (2022). "Stability and deformation responses of earth slopes subjected to multiple natural and manmade hazards." *International Journal of Geomechanics*, ASCE, **22**(3). https://doi.org/10.1061/(ASCE)gm.1943-5622.0002295

Wheeler, S. and Sivakumar, V. (1995). "An elasto-plastic critical state framework for unsaturated soil," *Géotechnique*, **45**(1), 35-53. https://doi.org/10.1680/geot.1995.45.1.35

World Meteorological Organization (WMO) (2021). "Weather-related disasters increase over past 50 years, causing more damage but fewer deaths." Retrieved 13 December 2021, from https://public.wmo.int/en/media/press-release/weather-related-disasters-increase-over-past-50-years-causing-more-damage-fewer

Yang, T., Zhang, Q., Zhang, X., Li, X., Zhang, J., Sun, Y., and Li, Z. (2019). "Cohesion variation during instability evolution of disaster medium in mud inrush of the mountain tunnel." *Journal of Mountain Science*, **16**(11), 2519-2531. https://doi.org/10.1007/s11629-019-5651-0